Roughening Rates of Strained-Layer Instabilities

Fumiya Watanabe, David G. Cahill, and J. E. Greene

Department of Materials Science and Engineering and the Frederick Seitz Materials Research Laboratory, University of Illinois at Urbana-Champaign, Urbana, Illinois, 61801, USA

(Received 10 November 2004; published 14 February 2005)

We study the evolution of the morphology of $Si_{0.75}Ge_{0.25}$ strained layers using a wide range of deposition times, $60 < \tau < 2400$ s, at 600 °C on laser textured substrates with miscuts $\theta < 15°$ off Si(001). Ripple-shaped morphologies form spontaneously on miscuts along the $\langle 110 \rangle$ directions. At the shortest deposition times, roughening is suppressed as predicted by a linear stability analysis that uses previously measured values for the mass transport rate on the surface. The measured time constant of the roughening is ≈ 80 s, a factor of 4 larger than predicted by theory.

DOI: 10.1103/PhysRevLett.94.066101 PACS numbers: 68.47.Fg, 68.35.Md, 68.55.Ac, 68.55.Jk

Instabilities of surface morphology play a key role in the synthesis and processing of crystalline layers that are elastically strained by a misfit between the lattice constant of the layer and the substrate [1]. The simplest manifestation of this instability of strained layers has been described independently by Asaro and Tiller, Grinfeld, and Srolovitz (ATGS): on a thermodynamically rough, i.e., nonfaceted orientation of a crystal, the morphology of a strained layer is linearly unstable and roughens spontaneously [2–4]. The rate at which the roughness evolves is controlled by the kinetics of mass transport on the surface and the thermodynamic driving forces of elastic strain energy and surface stiffness. The ATGS instability limits the use of planar strained layers in novel electronic device structures [5,6] and underlies the formation of epitaxial nanostructures in the Stranski-Krastanov growth mode [7–9].

To the best of our knowledge, however, the rate at which surface roughness develops in the ATGS instability, i.e., the roughening rate of the instability, has never been tested quantitatively by experiment. This lack of data can be attributed to two factors: (i) the kinetics of surface mass transport are known only in limited cases and (ii) most experiments use low-index orientations of the crystal that are not thermodynamically rough. The presence of a cusp in the surface free energy as a function of surface orientation introduces a nucleation barrier for roughening and the kinetics of crossing this nucleation barrier are typically unknown. The deposition of Si-Ge alloys on laser textured Si surfaces provides a way to overcome these two difficulties. We have previously measured the mass transport rate of Ge-covered Si(001) surfaces at 600 °C [10] and the mass transport rate of clean Si(001) is known at 670 °C [11]. Therefore, we can make a reliable estimate of the surface kinetics of a Si-Ge alloy at 600 °C by extrapolation. Laser texturing of Si(001) allows us to examine all crystal orientations within 15° of (001) in a single experiment [10,12,13]. Orientations with a large miscut in the $\langle 110 \rangle$ directions roughen without a nucleation barrier and enable quantitative tests of the roughening rate predicted by the ATGS theory.

Our work is also motivated by recent speculations concerning the effects of a high deposition flux in stabilizing the morphology of strained layers [8,9,14–16]. Layers deposited at high rates do not roughen significantly, but we argue that this lack of roughening can be simply attributed to the short time scale of the deposition: with a rapid deposition rate, a rough surface morphology does not have time to develop [14]. A planar layer deposited with a high deposition flux and then annealed for 600 s roughens to essentially the same degree as a layer that is deposited to the same thickness, only more slowly over the course of 600 s.

The ATGS analysis considers the competing changes in chemical potential created by an increase in surface area and relaxation of mechanical strain [1] and predicts an exponential roughening rate ω of a periodic surface morphology of wave number $q = 2\pi/\lambda$ [2,4],

$$\omega = \left(\frac{Dn_0\Omega^2}{k_B T}\right) q^3 \left(\frac{2\sigma_0^2}{M} - \tilde{\gamma} q\right), \qquad (1)$$

where D, n_0, and Ω are, respectively, diffusivity, concentration, and the volume of the adspecies responsible for mass transport on the surface. The product Dn_0 has units of inverse time, and we refer to this fundamental property of the surface as the mass transport rate. σ_0 is the layer stress, and $\tilde{\gamma}$ is the surface stiffness $\tilde{\gamma}(\theta) \equiv \gamma + \frac{\partial^2 \gamma}{\partial \theta^2}$. In the ordinary problem analyzed by ATGS, M is the plane strain modulus. In our experiments, the morphology is one dimensional, but the layers are under biaxial stress. We are not aware of an exact solution [15,17] to this geometry and set M equal to the biaxial modulus as an approximation.

For a surface profile of wave number q larger than a critical value, i.e., $q > q_c = 2\sigma_0^2/(M\tilde{\gamma})$, $\omega < 0$, roughening is suppressed, and the surface remains smooth. For $q < q_c$, $\omega > 0$, and a perturbation of the surface morphology of wave number q grows exponentially with the dependence $\exp(\omega\tau)$. The maximum roughening rate ω_m occurs at the "most unstable" wave number $q_m = 3\sigma_0^2/(2M\tilde{\gamma})$,

 © 2005 The American Physical Society

$$\omega_m = Dn_0\left(\frac{\Omega\sigma_0^2}{2Mk_BT}\right)\Omega q_m^3. \quad (2)$$

This mode is expected to dominate the surface morphology. Although q_m is inversely proportional to the surface stiffness $\tilde{\gamma}$, Eq. (2) predicts that the roughening rate of a mode with a fixed wave number q_m is independent of $\tilde{\gamma}$.

If a layer can be deposited in a time τ such that $\omega_m\tau \ll 1$, the instability of the morphology should be suppressed. For layers with high strain, ω_m is large and the short deposition time required to satisfy $\omega_m\tau \ll 1$ is not typically accessible to experiment. As we discuss below, $1/\omega_m$ for a strain $\epsilon = 0.01$ is on the order of 100 s; therefore, $\omega_m\tau \ll 1$ is accessible at high deposition rates if the strain in the layer is not too large.

Si(001) wafers with miscut of 0.1° toward $\langle 110\rangle$ are textured with a frequency-doubled pulsed yttrium-aluminum-garnet laser ($\lambda = 532$ nm) to create smooth craterlike dimples approximately 5 μm in diameter at the outer edge and 150 nm in depth at the center [18]. $Si_{0.75}Ge_{0.25}$ layers are grown from disilane and digermane precursors [10,13]. To ensure the cleanliness of the starting surfaces, we first deposit pure Si buffer layers, ~11 nm in thickness, at 800 °C [10]. The miscuts inside the dimples range $0° < \theta < 15°$ after the buffer layer growth. Layer thickness, given in equivalent monolayers (ML) of silicon (6.79×10^{14} cm^{-2}), and composition are measured by Rutherford backscattering spectrometry. The biaxial misfit strain of the $Si_{0.75}Ge_{0.25}$ epitaxial layers is 0.010. Surface morphologies are characterized by atomic force microscopy (AFM). Approximately 100 ML thick $Si_{0.75}Ge_{0.25}$ layers are grown at a fixed temperature of 600 °C, and the deposition times are varied by a factor of ≈ 45, from 60 to 2400 s, corresponding to deposition rates of 0.041 to 1.9 ML/s.

AFM images of the surface morphologies of ~100 ML thick layers of $Si_{0.75}Ge_{0.25}$ with varying deposition times are shown in Fig. 1. The miscuts θ inside the dimples after the deposition of the $Si_{0.75}Ge_{0.25}$ layer range from 0° at the center to maximum values of 10°–12° at a radius of 0.75 μm. The miscut angle is 5° near the outer edge of the image.

The morphologies of $Si_{0.75}Ge_{0.25}$ layers on vicinal Si(001) have an intricate dependence on miscut (θ) and azimuth (φ), but relatively large domains of θ and φ show similar behaviors. In particular, ripple-shaped morphologies at $5° < \theta < 12°$ miscut toward the $\langle 110\rangle$ directions dominate the fourfold symmetric patterns when the growth time τ exceeds 150 s.

The amplitudes of the ripple-shaped instabilities are strongly dependent on the deposition time; i.e., the instabilities are suppressed at the shortest deposition time. The average widths w and amplitudes z_0 of these ripple-shaped instabilities are plotted as a function of the layer deposition time τ in Fig. 2. The amplitudes are defined as $\frac{1}{2}$ of the valley-to-peak heights of the instabilities.

We fit the amplitudes z of the ripple-shaped morphologies produced by the five shortest growth times τ to $z_0 = z_m \exp(\omega_m\tau)$ with z_0 and ω_m as parameters. The best fit is obtained with $z_m = 0.036 \pm 0.024$ nm and $\omega_m = 0.012 \pm 0.002$ s^{-1} as shown with the dashed line in Fig. 2, corresponding to a characteristic time constant of $1/\omega_m \approx 80 \pm 13$ s. For the two shortest growth times, the upper limits of the amplitudes are considered in our fitting procedure, although ω_m values are not strongly affected by these data. For $\tau > 300$ s, the amplitudes deviate from the prediction of linear instability analysis which assumes that the thermodynamic driving force for roughening, i.e., the relaxation of elastic strain, increases linearly with the amplitude. The linear dependence of the driving force on amplitude is a good approximation for small values of the aspect ratio z_0/w but becomes a poor approximation for $z_0/w > 0.03$ [16].

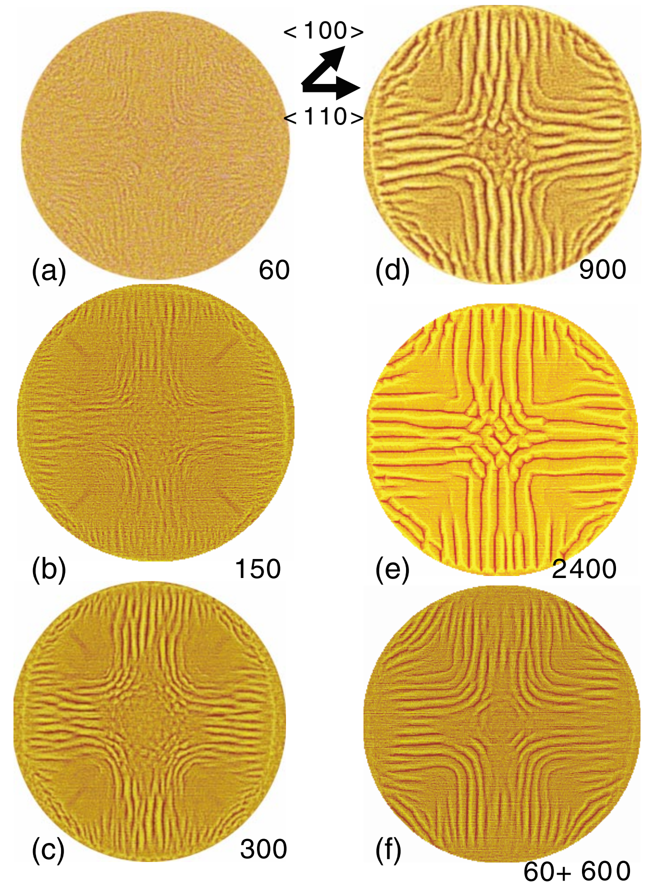

FIG. 1 (color online). Selected AFM micrographs of 100 ML thick $Si_{0.75}Ge_{0.25}$ layers grown with different layer deposition times. The images are high-pass filtered to separate the nanometer-scale features from the micron-scale curvature of the dimples. The numbers below each micrograph indicate the deposition time. For (f), 60 + 600 indicates 60 s deposition time and 600 s annealing time. The images are cropped near the top of the rim of the dimple. The diameter of each cropped image is ≈ 3 μm.

We now compare the experimental value for ω_m with the value of ω_m predicted by Eq. (2). To calculate ω_m from Eq. (2), we need the value of the mass transport rate, Dn_0, on the $Si_{0.75}Ge_{0.25}$ surface: for Ge on a Ge-wetting layer on Si(001) $Dn_0 = 1.5 \times 10^5\ s^{-1}$ at 600 °C [10]; for Si on Si(001) at 670 °C $Dn_0 = 3 \times 10^5\ s^{-1}$ [11]. Extrapolating the Si data [11] with an activation energy of ≈ 1.6 eV [19], we estimate $Dn_0 = 6.2 \times 10^4\ s^{-1}$ at 600 °C for Si on Si(001). The surface composition of the $Si_{0.75}Ge_{0.25}$ alloy during growth is not known exactly, and we do not know by how much the mass transport rate will vary with vicinality, but we expect that Dn_0 of our samples can be approximated by a geometric average of the limiting values for Si on Si(001) and Ge on a Ge-wetting layer on Si(001) and that the uncertainty in Dn_0 can be approximated by these same limits; therefore, we set $Dn_0 = (1.0 \pm 0.4) \times 10^5\ s^{-1}$. The mass transport rates are derived assuming that the diffusing species are dimers [10,11]. We are also assuming that the anisotropy in the mass transport rate is not pronounced. At low temperatures, on the order of 100 °C, the diffusion constants of Si-Si [20,21] and Si-Ge ad-dimers [22] on Si(001) are known to be highly anisotropic. (We note that the diffusion rates for Si-Si and Si-Ge ad-dimers are identical to within the experimental uncertainties [20,22].) Experiments on island nucleation [23] and island ripening [11], however, show that Dn_0 on single terraces of Si(001) is essentially isotropic at high temperatures, $T > 670$ °C [11,23].

At the transition from a smooth morphology to a rough morphology, the average width of the ripple-shaped morphology is $w \approx 80 \pm 10$ nm; see Fig. 2. We identify this length as the most unstable wavelength λ_m. Finally, using the biaxial modulus of the Si(001) substrate, $M = 180$ GPa in Eq. (2), $\omega_m \gg 0.06 \pm 0.03\ s^{-1}$ at $\epsilon = 0.010$, and the expected characteristic time $1/\omega_m \approx 20 \pm 10$ s, a factor ~4 smaller than the observed value. Since we are using the measured value of $q_m = 2\pi/\lambda_m$ in Eq. (2), ω_m does not depend on $\tilde{\gamma}$ and the uncertainty in ω_m is dominated by the uncertainties in Dn_0 and q_m.

We confirm that the observed ripple-shaped morphologies are not the result of kinetically driven step meanderings [24] by an annealing experiment. A smooth layer deposited with a 60 s deposition time was annealed for 600 s at 600 °C in UHV immediately following the layer deposition. The resulting morphology is similar to the morphology of the layer with a 300 s deposition time; see Fig. 1. The width and the amplitude of the ripple-shaped morphology formed by annealing are plotted as an open circle and an open square in Fig. 2; the data points for the annealed layer fall near the data for layers grown continuously over a comparable time. In this way, we confirm that the origin of the instability is thermodynamic and not caused by kinetic effects related to step motion.

The width of the ripple-shaped morphologies w varies weakly with growth time τ, and w appears to scale as $w \propto \tau^\eta$ with $\eta = 0.30 \pm 0.03$. Previous experiments [9] and theory [16] have also found that morphologies of strained layers coarsen with time. With shorter deposition times, less time is available for coarsening. Therefore, the width w of the instability should approach the characteristic wavelength λ_m at growth times comparable to the transition between smooth and rough growth.

The mechanism of coarsening is not known precisely, but intermixing of the layer atoms with those of the substrate and alloy decomposition within the layer should be considered [25]. At 600 °C, even a low deposition rate of 0.08 ML/s is sufficient to suppress intermixing between pure Ge layers and Si substrates [26]. The possibility of lateral alloy decomposition cannot be easily discounted. Previous reports of lateral alloy decomposition are for much lower deposition rates (0.0147 ML/s) [27] or much higher temperatures (720 °C) [28]. Samples grown with 0.8 ML/s at 520 °C did not show alloy decomposition [29]. A weak $\frac{1}{4}$ power-law dependence of the width of the ripple-shaped morphology on the deposition rate has been predicted by simulations that include lateral decom-

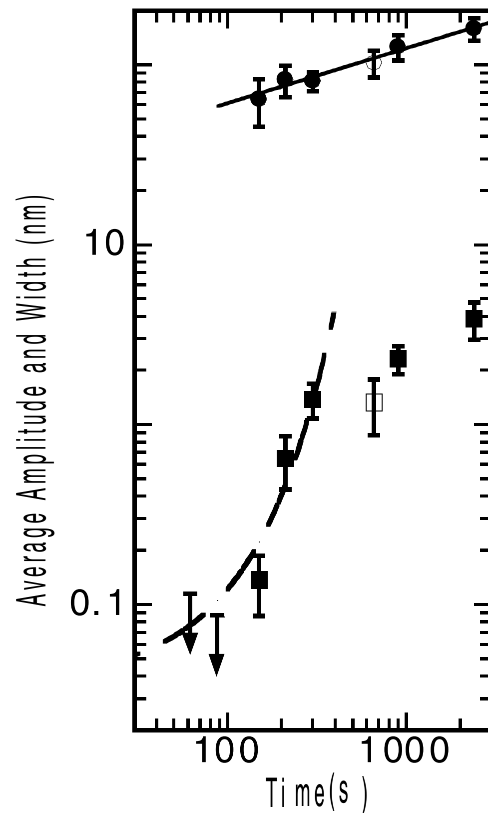

FIG. 2. Plot of average width (circles) and amplitudes (squares) of the ripple-shaped instability vs time. The error bars indicate the standard deviations in the measurements of ≈ 25 ripples. The widths have been corrected for ~5 nm overestimate due to the finite tip radius. The data from Fig. 1(f), 60 s deposition followed by 600 s anneal, are plotted as an open circle and an open square. The solid line indicates a 0.30 power-law fit to the instability widths. For the two shortest times, amplitudes are shown with bars and arrows pointing down to indicate the upper limit. An exponential function $z_0 = z_m \exp(\omega_m t)$ has been fit to the data, $z_m = 0.036$ nm and $\omega_m = 0.012\ s^{-1}$.

position of the alloy [30]. We note, however, that coarsening of an ensemble of 3D islands can show similar behavior [31].

The linear stability analysis we are using does not consider the influence of the growth flux in modifying the kinetics of mass transport on the surface. The validity of that approach can be addressed by the answer to the following question: during growth at 600 °C, does the flux of adatoms and dimers that are deposited on the surface significantly modify the equilibrium density of dimers that are responsible for mass transport? A quantitative answer to that question will depend on the average migration length of the dimers l, Dn_0, and the growth flux F. By dimensional analysis, we find $\Delta n/n_0 = Fl^2/(Dn_0)$, where Δn is the change in the ad-dimer density created by the growth flux. In our experiments, $F/(Dn_0)$ is approximately 10^{-5} in atomic units. If $l < 100$ lattice constants, then $\Delta n/n_0 \ll 1$. For growth of strained alloys on vicinal surfaces, we believe that $l < 100$ will be easily satisfied because of the high density of possible binding sites on the surface.

In addition to the ripple-shaped morphologies formed at high miscut toward the $\langle 110 \rangle$ directions, other features inside the dimples deserve mention. We also observe distinct regions with $\theta < 5°$ and miscuts toward $\langle 100 \rangle$ with $5° < \theta < 12°$. At longer deposition times, in the centers of the dimples at $\theta < 5°$ and at all φ, the instabilities have the fourfold symmetry of pyramidal shaped islands, commonly found in the other studies with low miscut substrates [7–9]. In regions with miscut toward the $\langle 100 \rangle$ directions, with $7° < \theta < 12°$, the morphology is relatively stable at all deposition rates [13]. The centers of these stable regions at $\theta \sim 11°$ are (105)-type facets which stay relatively flat even at the longest deposition time. We have not extensively studied growth of $Si_{0.75}Ge_{0.25}$ on vicinal planar substrates, but our prior work on the growth morphologies of highly strained GeSi alloy layers [13] and Ge low-temperature homoepitaxy [12,32] support our assertion that the morphologies observed within the curved dimpled substrate are characteristic and predictive of the morphologies that would be produced on planar Si wafers with the same vicinality.

In conclusion, textured substrates and a wide range of deposition times have enabled us to study the roughening rates of strained-layer instabilities. The morphologies on low strain layers are proven to be thermodynamic in origin and not the results of kinetic effects. Linear instability analysis is not only sufficient in describing the morphological changes in the layers qualitatively but also is adequate in deriving the quantitative rate of the roughening.

F. W. thanks N. Bartelt, B. Spencer, and V. Shenoy for helpful comments. This work was supported by the U.S. Department of Energy, Division of Materials Sciences under Contract No. DEFG02-91ER45439, through the Frederick Seitz Materials Research Laboratory at the University of Illinois. The sample characterization was carried out at the Center for Microanalysis of Materials, which is partially supported by the U.S. Department of Energy under Grant No. DEFG02-91-ER45439.

[1] D. G. Cahill, J. Vac. Sci. Technol. A **21**, S110 (2003).
[2] R. J. Asaro and W. A. Tiller, Metall. Trans. **3**, 1789 (1972).
[3] M. A. Grinfeld, Sov. Phys. Dokl. **31**, 831 (1986).
[4] D. J. Srolovitz, Acta Metall. **37**, 621 (1989).
[5] U. Konig and H. Dambkes, Solid-State Electron. **38**, 1595 (1995).
[6] S. E. Thompson *et al.*, IEEE Electron Device Lett. **25**, 191 (2004).
[7] J. A. Floro *et al.*, Appl. Phys. Lett. **73**, 951 (1998).
[8] P. Sutter and M. G. Lagally, Phys. Rev. Lett. **84**, 4637 (2000).
[9] R. M. Tromp, F. M. Ross, and M. C. Reuter, Phys. Rev. Lett. **84**, 4641 (2000).
[10] T. Schwarz-Selinger *et al.*, Phys. Rev. B **65**, 125317 (2002).
[11] N. C. Bartelt, W. Theis, and R. M. Tromp, Phys. Rev. B **54**, 11741 (1996).
[12] A. Raviswaran and D. G. Cahill, Phys. Rev. B **69**, 165313 (2004).
[13] F. Watanabe *et al.*, Appl. Phys. Lett. **85**, 1238 (2004).
[14] B. J. Spencer, P. W. Voorhees, and S. H. Davis, Phys. Rev. Lett. **67**, 3696 (1991).
[15] L. B. Freund and F. Johnsdottir, J. Mech. Phys. Solids **41**, 1245 (1993).
[16] R. V. Kukta and L. B. Freund, J. Mech. Phys. Solids **45**, 1835 (1997).
[17] H. Gao, J. Mech. Phys. Solids **42**, 741 (1994).
[18] T. Schwarz-Seilinger *et al.*, Phys. Rev. B **64**, 155323 (2001).
[19] J. Erlebacher *et al.*, Phys. Rev. Lett. **84**, 5800 (2000).
[20] B. S. Swartzentruber, Phys. Rev. Lett. **76**, 459 (1996).
[21] B. Borovsky, M. Krueger, and E. Ganz, Phys. Rev. B **59**, 1598 (1991).
[22] X. R. Qin, B. S. Swartzentruber, and M. G. Lagally, Phys. Rev. Lett. **85**, 3660 (2000).
[23] R. M. Tromp and M. Mankos, Phys. Rev. Lett. **81**, 1050 (1998).
[24] C. Schelling, G. Springholz, and F. Schaffler, Phys. Rev. Lett. **83**, 995 (1999).
[25] J. E. Guyer and P. W. Voorhees, Phys. Rev. Lett. **74**, 4031 (1995).
[26] M. Floyd *et al.*, Appl. Phys. Lett. **82**, 1473 (2003).
[27] D. D. Peroivc *et al.*, Physica (Amsterdam) **239A**, 11 (1997).
[28] T. Walther, C. J. Humphreys, and A. G. Cullis, Appl. Phys. Lett. **71**, 809 (1997).
[29] I. Berbezier *et al.*, Surf. Sci. **412**, 415 (1998).
[30] F. Leonard and R. C. Desai, Appl. Phys. Lett. **74**, 40 (1999).
[31] P. Wynblatt and N. A. Gjostein, in *Progress in Solid State Chemistry*, edited by J. O. McCaldin and G. Somorjai (Pergamon, Oxford, 1975), Vol. 9.
[32] J. E. Van Nostrand, S. J. Chey, and D. G. Cahill, Phys. Rev. B **57**, 12 536 (1998).